JOURNAL OF CATALYSIS 137, 212–224 (1992)

Fischer–Tropsch Synthesis on Cobalt and Ruthenium. Metal Dispersion and Support Effects on Reaction Rate and Selectivity

ENRIQUE IGLESIA,[1] STUART L. SOLED, AND ROCCO A. FIATO[2]

Corporate Research Laboratories, Exxon Research and Engineering Co., Route 22 East, Annandale, New Jersey 08801

Received February 14, 1992; revised April 23, 1992

Metal dispersion and support effects on Fischer–Tropsch synthesis rate and selectivity were studied at conditions that favor the information of C_5+ hydrocarbons (> 80% selectivity). On Ru, these effects are minor for the supports (SiO_2, Al_2O_3, TiO_2) and the dispersion range (0.0009–0.60) tested. Site-time yields are similar ($1.25–1.95 \times 10^{-2}$ s^{-1}) on all Ru catalysts (476 K, 560 kPa, $H_2/CO = 2.1$). On Co, hydrocarbon synthesis rates are also proportional to metal dispersion (0.0045–0.095) and independent of the metal oxide support (SiO_2, Al_2O_3, TiO_2, and ZrO_2-modified SiO_2 and TiO_2). Site-time yields ($1.6–3.0 \times 10^{-2}$ s^{-1}) are independent of Co dispersion and support (473 K, 2000 kPa, $H_2/CO = 2.1$). Dispersion and support influence C_5+ selectivity slightly on both Co and Ru catalysts; these changes reflect transport-enhanced secondary reactions and not modifications of intrinsic chain growth kinetics. Specifically, transport restrictions imposed by the physical structure of the support and by a high site density within catalyst pellets increase the residence time and the readsorption probability of reactive α-olefins and lead to higher C_5+ yields and more paraffinic products.

I. INTRODUCTION

CO hydrogenation is a critical step in the synthesis of paraffins, olefins, and oxygenates from natural gas. When operating conditions and catalyst composition lead to high molecular weight hydrocarbons, this reaction is known as the Fischer–Tropsch synthesis (1). Overall process efficiency requires catalysts with high volumetric productivity, high C_5+ yields, and low selectivity to methane and other light hydrocarbons.

Catalytic rates and selectivity can reflect the intrinsic behavior of a metal surface. Sometimes, this surface chemistry changes because metal crystallites of different size expose surface ensembles with unique structure (2); strong interactions with a metal oxide support can also perturb the electronic density and structure of metal crystallites (3). Here, we explore how metal crystallite size (dispersion) and metal-support interactions affect the intrinsic reactivity of Co and Ru surfaces in the Fischer–Tropsch synthesis. Although many previous studies have addressed this important issue, published reports disagree on the existence and even on the directionality of dispersion and support effects in CO hydrogenation catalysis. Moreover, many studies were conducted at low reactant pressures and high temperatures, which favor methanation over Fischer–Tropsch synthesis and which also lead to extensive secondary reactions and deactivation.

Catalytic CO hydrogenation occurs on metal sites (e.g., Co, Ru, Fe) located within porous solids that are frequently saturated with the liquid products of the synthesis reaction. As a result, slow transport of reactants (4–6) to and products (5–8) from catalytic sites often controls the rate of primary and secondary reactions even on small

[1] To whom correspondence should be addressed.

[2] Current address: Exxon Research and Engineering Co., 180 Park Ave., Florham Park, NJ 07932.

0021-9517/92 $5.00

catalyst pellets. In the particle size range used in our studies (< 0.20 mm pellet diameter), transport limitations modify only selectivity. Readsorption of α-olefins is enhanced as the density of readsorption sites increases and as diffusional restrictions imposed by the pellet size and the pore structure limit intrapellet olefin removal rates; α-olefin readsorption leads to heavier more paraffinic products (*7*, *8*). Detailed models that account for intrapellet transport restrictions to reactant arrival and product removal were reported previously (5–7). The models describe changes in C_5+ selectivity caused by dispersion and support effects, differences that do not arise from changes in intrinsic surface chemistry but rather from physical transport processes that affect Fischer–Tropsch selectivity even on small pellets (<0.2 mm diameter).

Here, we examine the structure-sensitivity of CO hydrogenation on cobalt and ruthenium crystallites supported on high-purity SiO_2, Al_2O_3, TiO_2, and other supports at Fischer–Tropsch synthesis conditions that lead to high C_5+ selectivity (> 80%). We conclude that synthesis rates are proportional to the density of Co and Ru surface atoms. Site-time yields do not depend strongly on the metal crystallite size or on the identity of the metal oxide support. Intrinsic surface chemistry is not strongly affected by any surface modifications caused by changes in metal crystallite size or by interactions between metal and support. Therefore, improved catalysts will require materials with high volumetric site densities, because neither the identity of the support nor the crystallite size significantly increase the intrinsic catalytic activity of exposed Co and Ru atoms.

II. EXPERIMENTAL

A. Catalyst Synthesis and Characterization

Ru catalysts were prepared by incipient wetness impregnation of TiO_2 (P25, Degussa, 60–75% rutile), SiO_2 (Davison, Grade 62; Shell spheres, S980A-G), and γ-Al_2O_3 (Catapal SB, Conoco) with a solution of Ru nitrate (Engelhard Corp.) in acetone. The supports were calcined in air at 873 K for 1–4 h before impregnation. The rutile content in TiO_2 supports was 20–30% in the untreated Degussa P25 material and about 60–75% in the calcined samples. A sample of pure anatase TiO_2 was prepared by hydrolysis of Ti isopropoxide and calcination at 673 K for 2 h. The impregnated samples were dried by slow evaporation at room temperature and then evacuated at 373 K overnight. The unsupported Ru powder was obtained from Johnson–Mathey (Puratronic grade). Cobalt catalysts were prepared similarly using an aqueous Co nitrate solution (Johnson Mathey, Puratronic grade).

The ZrO_2/SiO_2 support was prepared by impregnation of SiO_2 with a zirconium salt, using procedures reported previously (*9*). The $Zr_{0.14}Ti_{0.86}O_2$ mixed-metal oxide support was prepared by hydrolysis of a mixed alkoxide solution (*10*). The resulting precipitate was filtered, dried, and calcined at 973 K for 2 h. The sample retained the anatase structure even after the calcination treatment.

All samples were sieved in order to obtain desired pellet sizes (80–140 mesh, 0.17-mm average diameter). Co catalysts were cal cined in air between 373 and 773 K for 2–4 h before reduction. All catalysts were reduced in flowing dihydrogen at 723 K for 4 h and passivated with a dilute (1%) oxygen stream. The samples were reduced again at 673 K for 1–3 h before chemisorption and catalytic measurements.

Ru, Co, Cl, and alkali concentrations were measured by atomic absorption or X-ray fluorescence. Cl (<200 ppm) and Na (<50 ppm) concentrations were very low on all catalysts. Metal crystallite sizes were calculated from transmission electron micrographs and from the breadth of Co metal X-ray diffraction lines using the Scherrer equation. The rutile content in TiO_2 was determined from the relative intensities of the rutile and anatase X-ray diffraction lines using CuKα radiation. Physical surface areas

and pore size distributions were determined by N_2 adsorption (*11*). The extent of reduction of supported Co precursors was measured by oxygen uptake measurements at 673 K after reduction, assuming the formation of Co_3O_4 during oxidation (12).

The ruthenium dispersion, defined as the fraction of metal atoms residing at the surface of supported metal crystallites, was measured at 373 K by titrating oxygen preadsorbed at 170 K with dihydrogen (7). The stoichiometries for hydrogen titration of chemisorbed oxygen,

$$2\,H_2 + Ru_2 - O \xrightarrow{(373\ K)} 2\,Ru - H + H_2O, \quad (H/Ru)_s = 2.0, \quad (1)$$

and for oxygen titration of chemisorbed hydrogen,

$$2\,O_2 + 4\,Ru - H \xrightarrow{(170\ K)} 2\,Ru_2 - O + H_2O, \quad (O/Ru)_s = 1.0, \quad (2)$$

were established by measurements on Ru powder and on supported samples with known Ru crystallite size (from TEM). Similar results were obtained by titrating adsorbed oxygen with H_2 (Eq. (1)) or adsorbed hydrogen with O_2 (Eq. (2)). These titration methods give accurate values of exposed metal in TiO_2-supported samples, regardless of reduction temperature or SMSI behavior.

The cobalt dispersion was measured by hydrogen chemisorption at 373 K, assuming a 1:1 H:Co surface stoichiometry (*13, 14*). Prereduced Co/TiO_2 catalysts were heated in air at 573 K for 0.5 h and re-reduced at 523 K in H_2 before chemisorption experiments. Such a treatment was required in order to avoid strong metal–support interactions (SMSI) that strongly inhibit CO and H_2 chemisorption (*3*). These metal dispersions were used to calculate the density of exposed metal atoms in supported catalysts and to report reaction rates as site-time yields or turnover rates.

B. Catalytic Measurements

Steady-state hydrocarbon synthesis rates and selectivities were measured in an isothermal fixed-bed reactor at 473 K, 560–2000 kPa, and H_2/CO reactant ratios near stoichiometric consumption values (2.05–2.1). Catalysts were reduced in H_2 at 673 K for 1–3 h, cooled to synthesis temperature, and exposed to CO and H_2 reactants. All reported data were obtained after at least 24 h on stream in order to ensure steady-state behavior and complete pore filling by liquid reaction products. Catalytic data were obtained over a wide range of CO conversions (5–80%) by varying the space velocity at constant temperature and pressure. We choose to report rate and selectivity data at integral reactor conditions (45–60% CO conversion) instead of differential conditions (<10% conversion) in order to maximize the contribution of C_5+ hydrocarbons to the product yield. All comparisons are made at similar conversions and our conclusions remain valid when similar comparisons are made at lower CO conversions.

The reactor effluent was analyzed directly (C_1–C_{15}, CO, CO_2) and after product collection ($C_{16}+$) by gas chromatography using flame ionization, thermal conductivity, and mass spectrometric detection with N_2 as an internal standard. The carbon number distribution of $C_{35}+$ products was determined by high-temperature gas chromatography and gel-permeation chromatography (*7*). Selectivities are reported on a carbon basis as the percentage of converted CO that appears as a given product. Synthesis rates are reported both as a metal-time yield (moles CO converted/g-atom metal-s) and as a site-time yield or turnover rate (moles CO converted/g-atom surface metal-s). Site-time yields were measured on catalyst pellets with average diameters less than 0.2 mm in order to avoid diffusion-limited CO conversion at catalytic sites.

C. Chain Growth and Product Distributions

In Fischer–Tropsch synthesis, chain growth occurs by stepwise addition of a C_1 monomer to a surface alkyl group (*15, 16*). Chain termination occurs by hydrogen ab-

straction or addition to form olefins and paraffins, respectively. Olefins can readsorb and initiate surface chains in a step that reverses the hydrogen abstraction termination step. Secondary hydrogenation of olefins can also occur at very low CO pressures or on catalysts containing a catalytic hydrogenation function that is not inhibited by the presence of CO.

Mathematical treatments developed for polymerization processes are well suited to describe product distributions in the Fischer–Tropsch synthesis. Flory carbon number distributions (*17, 18*),

$$S_n = n \cdot (1 - \alpha)^2 \cdot \alpha^{n-1}, \qquad (3)$$

where S_n is the carbon selectivity for chains with n carbon atoms, are obtained when the chain growth probability (α) is independent of chain size. A plot of ln (S_n/n) vs n gives a straight line when α is independent of n. A more general treatment allows for chain growth kinetics that depend on chain size. In this approach, the termination probability for a given chain size is calculated using (*19*)

$$\beta_n = \frac{r_{t,n}}{r_{p,n}} = \left(1 - \frac{1}{\alpha_n}\right) = \phi_n \Big/ \sum_{i=n+1}^{\infty} \phi_i, \qquad (4)$$

where ϕ_n is the mole fraction of chains of size n and $r_{t,n}$ and $r_{p,n}$ are their termination and propagation rates, respectively. The denominator in Eq. (4) requires that we accurately measure the entire product distribution. The chain termination probability is a linear combination of the net values for each termination step; these net values include the rates of both forward and reverse steps. For example, if chains terminate to paraffins ($\beta_{H,n}$) and olefins ($\beta_{o,n}$) and the latter readsorb and initiate surface chains ($\beta_{r,n}$), the total chain termination probability is given by

$$\beta_{T,n} = \beta_{H,n} + (\beta_{o,n} - \beta_{r,n}) \qquad (5)$$

III. RESULTS AND DISCUSSION

A. Catalyst Characterization

Metal content and dispersion data on Ru and Co catalysts are reported in Tables 1 and 2. The measured dispersions agree well with those calculated from X-ray diffraction line broadening and transmission electron microscopy. The latter two techniques give an average particle size that must be converted to a dispersion value by assuming a crystallite shape (hemispherical, in this case), whereas chemisorption gives a direct measurement of exposed metal atoms. The agreement between site titration and physical characterization techniques extends to strongly interacting supports, such as TiO_2, when the SMSI state is destroyed by an air treatment before chemisorption measurements or by the H_2–O_2 titration procedure itself.

The Ru and Co species present in these catalysts are predominantly zero-valent. Temperature-programmed reduction and oxygen uptake measurements show that more than 90% of the Co atoms in these samples are reduced to metal during the hydrogen pretreatment.

B. Metal Dispersion and Support Effects on Ru

Specific CO hydrogenation rates (metal-time yields) increase linearly with Ru dispersion (Fig. 1). Site-time yield values lie within a narrow range ($1.25–1.95 \times 10^{-2}$ s^{-1}) on all Ru catalysts, including unsupported powders (Table 1). Therefore, support and dispersion effects on reaction rate are minor for the supports (SiO_2, Al_2O_3, TiO_2) and dispersions (0.0009–0.60) used in this study. Moreover, site-time yields are independent of TiO_2 crystal structure and of catalyst reduction temperature. Thus, CO hydrogenation rates are proportional to the number of exposed Ru surface atoms and independent of crystallite size, support identity, or strong metal–support interactions. The SMSI state is apparently destroyed by exposure to the water product of the Fischer–Tropsch synthesis; SMSI effects do not appear to influence catalytic rates at our reaction conditions.

Carbon number distributions are qualitatively similar on all Ru catalysts tested. Termination probabilities (β_n) for short chains

TABLE 1

Elemental Composition, Dispersion, and Catalytic Properties of Ru Catalysts

Support	Ru content (wt. %)	Ru dispersion[a]	Ru-time yield ($10^3 \cdot s^{-1}$)[b]	Site-time yield ($10^3 \cdot s^{-1}$)[b]	Carbon selectivity (%)	
					CH_4[b]	C_5+[b]
TiO_2 (30% anatase)	1.2	0.48	6.8	13.0	3.7	87.3
TiO_2 (60% anatase)	0.9	0.60	7.5	12.5	5.0	84.0
TiO_2 (100% anatase)	4.8	0.26	4.2	16.1	3.0	89.0
SiO_2	10.6	0.22	2.5	11.4	4.2	89.1
SiO_2	1.8	0.082	1.3	15.8	8.1	71.6
γ-Al_2O_3	5.1	0.25	3.5	14.0	5.0	88.0
—	100	0.0009	0.018	19.5	2.0	95.0

[a] From hydrogen titration of chemisorbed oxygen.
[b] 476 K, 560 kPa, $H_2/CO = 2.1$, 45–60% CO conversion, 0.17-mm average pellet diameter.

($n < 20$) vary with Ru dispersion and support but reach similar asymptotic values for larger chains (Fig. 2). Chain termination probabilities decrease with increasing chain size on all catalysts. This reflects an increase in readsorption rate as α-olefins become larger and more difficult to remove from liquid-filled catalyst pellets (5–8). This behavior results in curved semilogarithmic plots (Eq. (3)). As olefins disappear from the product stream because of extensive readsorption ($n > 20$), the chain termination probability reaches a constant value and Flory plots become linear. The asymptotic value of the chain termination probability (β_n) in this region reflects the intrinsic probability of chain termination to paraffins by hydrogen addition to growing alkyl chains. This intrinsic termination probability is independent of support and of Ru dispersion (Fig. 2).

The apparent effect of support and dispersion on chain termination (Fig. 2) and C_5+ selectivity (Table 1) arises from physical transport effects that occur even on small liquid-filled pellets; transport effects depend on the physical structure of the support and on the density of sites available for readsorption and chain initiation by α-olefins. As we discuss below, the slight differences in C_5+ selectivity among these catalysts can be described entirely by such transport effects and do not require different chain growth kinetics.

The structure insensitivity of CO hydrogenation reactions on Ru was initially suggested by Dalla-Betta *et al.* (20). They reported that initial CO hydrogenation rates were independent of Ru crystallite diameter (1–9 nm). In contrast, other groups report that CO hydrogenation rates increase with increasing crystallite size in a similar Ru dispersion range (*21, 22*). King (*21*) found that methanation turnover rates decreased from 0.16 to 0.01 s^{-1} as the Ru dispersion increased from near zero (unsupported) to 0.64; a significant decrease in turnover rate occurred in a dispersion range (from near 0 to 0.25) where changes in the surface density of low-coordination surface atoms are minor and where crystallite size is unlikely to influence strongly surface reactions (*2*). Kell-

TABLE 2

Elemental Composition, Dispersion, and Catalytic Properties of Co Catalysts

Support	Co content (% wt)	Cobalt dispersion			Co-time yield ($10^4 \cdot s^{-1}$)[c]	Site-time yield ($10^3 \cdot s^{-1}$)[c,d]	Carbon selectivity	
		Chemisorption[a]	TEM[b]	XRD[b]			CH_4	C_5+
TiO_2[e]	11.6	0.012	—	—	2.8	23.1	8.1	81.5
TiO_2[e]	11.9	0.022	—	—	5.0	22.7	6.8	84.5
TiO_2[e]	10.5	0.029	—	—	7.5	25.9	—	83.0
TiO_2[e]	12.1	0.053	—	—	11.4	21.5	—	—
TiO_2[e]	11.6	0.030	0.036	—	8.9	29.6	7.0	82.5
TiO_2[e]	11.8	0.065	0.073	0.056	15.3	23.5	5.4	90.1
SiO_2	24.8	0.042	—	—	11.3	27.0	4.7	91.0
SiO_2	23.1	0.032	0.036	0.039	6.7	20.8	6.3	85.5
SiO_2	14.0	0.019	—	—	3.4	17.5	7.5	84.0
SiO_2	15.0	0.050	—	—	13.1	26.1	7.0	83.5
SiO_2	13.0	0.063	—	—	16.7	26.5	5.8	89.6
SiO_2	15.0	0.060	0.081	—	14.7	24.5	6.4	85.2
SiO_2	10.3	0.095	0.079	—	20.2	20.7	5.3	88.5
SiO_2	32.1	0.0045	—	—	1.2	27.8	7.4	83.0
11.0% ZrO_2/SiO_2	17.2	0.061	—	—	10.0	16.4	5.6	84.0
$Zr_{0.14}Ti_{0.86}O_2$	10.6	0.011			3.1	27.5	8.2	83.2
Al_2O_3	19.5	0.036	0.045	0.031	6.9	19.2	7.8	82.5
Al_2O_3	11.2	0.015	—	—	2.4	16.0	8.7	80.2

[a] H_2 chemisorption uptake at 373K.
[b] From volume-averaged crystallite size.
[c] 473 K, 2000 kPa, H_2/CO = 2.1, 50–63% CO conversion, 0.17-mm average pellet diameter.
[d] Based on dispersion values from hydrogen chemisorption.
[e] 25–40% anatase, balance rutile.

ner and Bell (*22*) also reported a decrease in turnover rate with increasing metal dispersion on Ru/Al_2O_3 catalysts. Similar effects were observed at 0.1 and 1 MPa reactant pressures (H_2/CO = 3). Methane turnover rates at 498 K and 1 MPa decreased from 3×10^{-3} to 4×10^{-4} s^{-1} as the Ru dispersion increased from 0.25 to 0.80 (*22*). Smith and Everson (*23*) have also reported a tenfold decrease in turnover rate as the dispersion of 0.5% Ru/Al_2O_3 eggshell catalysts increased from 0.16 to 0.78. However, C_5+ selectivity and chain growth probability increased only slightly with decreasing Ru dispersion, a surprising result because methanation and chain growth are unlikely to involve rate-limiting surface steps with similar structural requirements.

Reported CO hydrogenation turnover rates on Ru(001) and Ru(110) single crystals

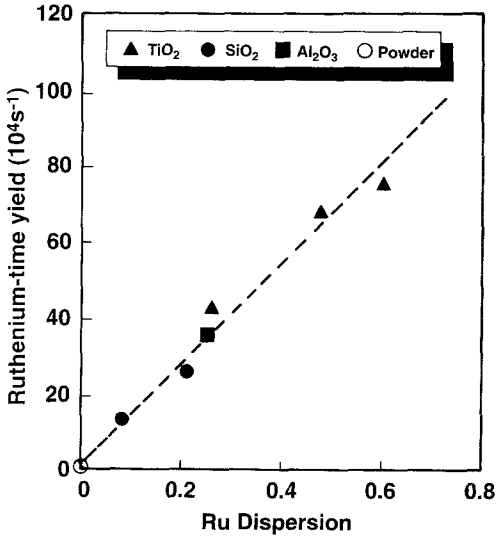

FIG. 1. Effects of ruthenium dispersion on Fischer–Tropsch synthesis rates (476 K, H_2/CO = 2.1, 560 kPa, 45–60% CO conversion).

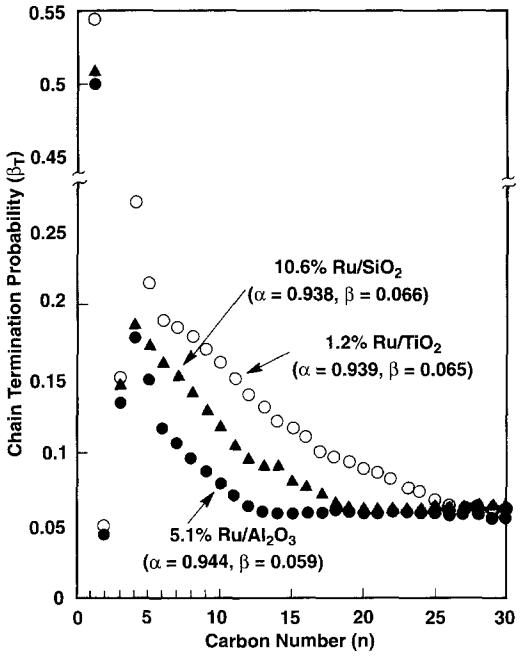

FIG. 2. Support effects on chain termination probability, ruthenium catalysts (476 K, H_2/CO = 2.1, 560 kPa, 45–60% CO conversion).

are similar and resemble those on supported Ru catalysts (*24*). These data suggest that methanation pathways and surface kinetics do not depend on the local structural details of the surface. Some reported alloy effects are consistent with structure insensitive pathways requiring small ensembles of Ru surface atoms. For example, alloying Ru crystallites with inactive Cu atoms led only to a modest initial decrease in turnover rate (*25*). Titration of sites with slightly higher specific activity by Cu atoms on nonuniform Ru surfaces probably accounts for this modest alloy effect. In another study, turnover rates did not change as the fraction of surface Cu on an Ru(001) single crystal increased, also suggesting a small ensemble requirement (isolated Ru atoms) (*26*). Much larger ensembles (4–13 Ru atoms), however, were suggested in earlier studies on Ru–Cu alloys (*27, 28*).

Vannice and Garten (*29*) found that methanation turnover rates on Ru did not depend on the identity of the support; however, the product molecular weight was significantly higher on TiO_2 than on other metal oxides. Kikuchi *et al.* (*30*) reported less than a twofold decrease in CO hydrogenation rate when Al_2O_3 replaced TiO_2 as the support for Ru crystallites (0.07–0.19 Ru dispersion, 523 K, 100 kP H_2/CO = 2). The chain growth probability was unaffected by the chemical identity of the support. In contrast, Stoop *et al.* (*31*) observed dramatic rate and selectivity differences among supports. These authors concluded that these differences did not reflect intrinsic support effects on Ru surface chemistry but the effect of Cl and other support impurities on active site density and chain growth probability (*31*).

Our results show that the synthesis of high molecular weight hydrocarbons does not depend strongly on the dispersion of Ru crystallites or on the identity of the metal oxide on which they are supported. These data were obtained on steady-state catalysts (>24 h on stream) at conditions where the C_5+ selectivity (> 80%) and the chain growth probability (0.94–0.95 for $C_{25}+$) were much higher than in previous studies. Our results suggest that the synthesis of high molecular weight hydrocarbons on Ru is a structure-insensitive reaction.

This structure insensitivity could be an intrinsic property of Fischer–Tropsch chemistry and reflect a rate-limiting surface step that does not depend on local surface structure or on available ensemble size. More probably, the structure insensitivity arises because chain growth occurs on surfaces covered almost completely by CO reactive intermediates, a mechanistic detail reflected in the negative CO pressure order of the Fischer–Tropsch synthesis. As a result, chain growth occurs only on a few surface sites (*32*), generally those that bind CO least strongly in structurally nonuniform but well-covered metal surfaces. Well-covered surfaces hide many of the structural features and specific binding sites initially present on the clean metal surface. Iglesia and Boudart

(*33*) previously proposed that, in general, catalytic reactions occurring on well-covered surfaces become structure insensitive for similar reasons. Similar arguments would suggest that the Fischer–Tropsch synthesis on fully reduced Co surfaces at normal CO partial pressures will also be insensitive to dispersion and support effects. The results in the next section confirm this suggestion.

In catalytic rate measurements, we probe the structural requirements of intermediates and of chemical reactions involved in the rate-limiting steps of a catalytic sequence. Thus, many of the contradicting reports of dispersion and support effects may reflect different operating conditions, which can alter the identity and the structural requirements of the rate-limiting step.

Previously reported dispersion and support effects on Ru catalysts were obtained at conditions that favor formation of light products, especially methane. In our study, we have extended this work to Fischer–Tropsch synthesis conditions where C_5+ selectivities exceed 80%. We conclude that synthesis of higher molecular weight hydrocarbons on Ru is structure-insensitive according to the definition given in Refs. (*34, 35*). Site-time yields and chain growth kinetics depend only weakly on Ru dispersion and on the identity of the metal oxide support.

C. Metal Dispersion and Support Effects on Co

The rate of hydrocarbon synthesis from H_2 and CO on Co catalysts is also proportional to the number of exposed metal atoms (Fig. 3). Cobalt-time yields increase linearly with increasing dispersion of Co crystallites (0.0045–0.095) supported on SiO_2, Al_2O_3, TiO_2, $Zr_{0.14}Ti_{0.86}O_2$, and ZrO_2/SiO_2. Site-time yields are $1.6 - 3.0 \times 10^{-2}\ s^{-1}$ at 2000 kPa and 473 K and do not depend strongly on support or metal dispersion (Table 2). These values suggest an upper limit of about 50 s for the time required to form a carbon–carbon bond; this limit is reached if

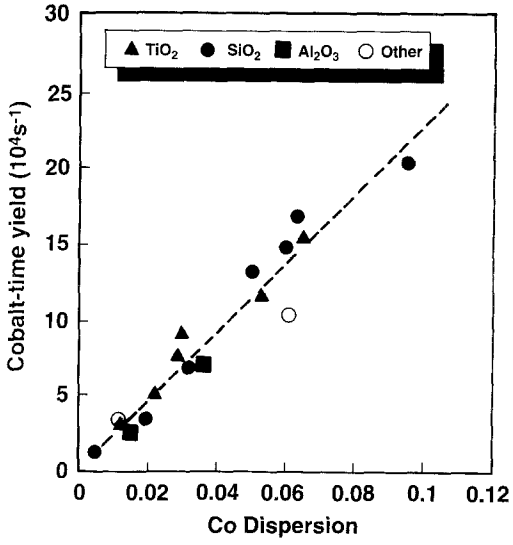

FIG. 3. Effects of cobalt dispersion on Fischer–Tropsch synthesis rates (473 K, H_2/CO = 2.1, 2000 kPa, 50–60% CO conversion).

every Co surface atom contains a growing chain. In this dispersion range (0.0045–0.095), site activity is not strongly affected by metal-support interactions or by crystallite size.

Carbon number distributions are similar on all Co catalysts (Fig. 4). As on Ru, product distributions are non-Flory; the observed curvature shows that chain growth probability increases with molecular size. The modest effects of support and dispersion on the carbon number distribution (Fig. 4) and on the C_5+ selectivity (Table 2) reflect differences in readsorption site density and in support pore structure (*5–8*); the latter controls the rate of removal of reactive olefins from catalyst pellets. Carbon number plots become linear for $C_{20}+$ hydrocarbons on all cobalt catalysts. The chain growth probability reaches a constant value (α_∞) as olefins disappear from the product stream. This constant value reflects the intrinsic probability of chain termination to paraffins by hydrogen addition; as on Ru catalysts, α_∞ is independent of support and of metal dispersion (Fig. 4).

The structure-insensitivity of CO hydrogenation on Co was recently proposed for

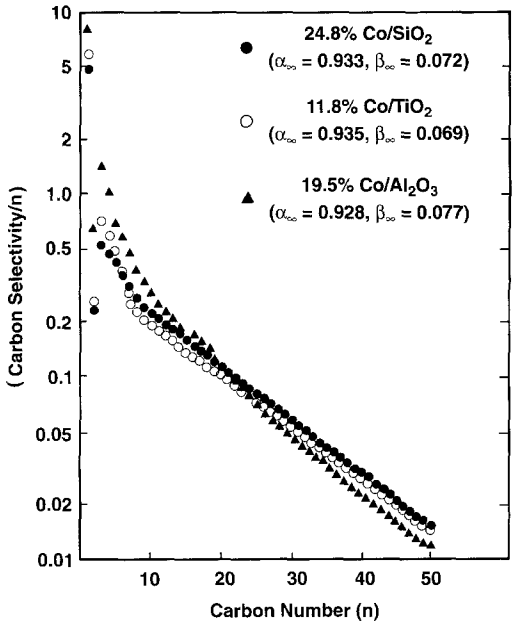

FIG. 4. Support effects on carbon number distribution, cobalt catalysts (473 K, H_2/CO = 2.1, 2000 kPa, 50–60% CO conversion).

SiO_2-supported catalysts with 0.06–0.22 Co dispersion (*36*). Turnover rates remained nearly constant (0.0018–0.0027 s^{-1}) over the entire dispersion range but neither reaction kinetics nor product distributions were reported. These catalysts were tested at 455 K and very low H_2/CO pressure (3 kPa CO, 9 kPa H_2), conditions far removed from normal Fischer–Tropsch synthesis and which led to turnover rates 10 times smaller than those reported here. At such low reactant pressures, methane is the predominant product and kinetics often become positive order in CO pressure, suggesting that the surface is no longer covered entirely by CO reactive intermediates. Thus, these findings (*36*) may agree only coincidentally with the similar structure insensitivity that we report here for the synthesis of higher hydrocarbons on Co. These authors also showed that Co dispersions measured by hydrogen chemisorption at 473 K agree well with values obtained by direct surface composition analysis of supported Co catalysts using ESCA (*36*).

Many previous reports had suggested strong crystallite size and support effects on the rate and selectivity of CO hydrogenation on Co (*37, 38*). Fu and Bartholomew (*38*) reported a sevenfold increase in turnover rate as Co dispersion decreased from 0.3 to 0.15; they concluded that CO hydrogenation (100 kPa, 473–523 K, H_2/CO = 2) on Co/Al_2O_3 is structure-sensitive and requires sites where CO is strongly coordinated. They proposed that the density of these strong binding sites and the nature of reactive CO species depend strongly on cobalt crystallite size. Similarly, they suggested that the higher molecular weight products observed on larger Co particles reflected crystallite size effects on intrinsic surface chain growth kinetics. Bartholomew and Reuel (*37*) also reported strong support and dispersion effects at similar reaction conditions. Turnover rates decreased in the order $TiO_2 > SiO_2 > Al_2O_3 > C$, MgO and with increasing dispersion on all supports. These dispersion and support effects were accompanied by incomplete reduction of the Co oxide precursors, a factor that strongly influences CO hydrogenation rates (*39*). These apparent dispersion and support effects may result from partially reduced Co sites that chemisorb hydrogen but do not catalyze Fischer–Tropsch synthesis or from sites that reoxidize readily in the presence of water during reaction. Similar phenomena may also account for the reported increase in turnover rate with increasing Co crystallite size (and extent of reduction) on Al_2O_3 surfaces (*40*), in a dispersion range (0.009–0.076) where surface structure is largely independent of crystal size (*2*).

Recent reports also suggest that the apparent strong structure-sensitivity of CO hydrogenation reactions on Co reflects differences in extent of reduction and in the ease of reoxidation of Co as a function of metal dispersion and of the chemical identity and surface properties of the metal oxide support. Johnson *et al.* (*41*) recently reported similar turnover rates on strained Co overlayers on W(110) and W(100) sub-

strates, even though the local geometry of the cobalt surface differs markedly on the two substrates. These turnover rates resembled those on Co sites supported on dehydroxylated Al_2O_3 surfaces, where Co oxide precursors were completely reduced to Co metal. On such supports, turnover rates were independent of dispersion for Co/Al_2O_3 catalysts with 0.05–0.37 dispersion (*41*). These authors also suggested that CO hydrogenation to methane is a facile reaction that proceeds with similar turnover rate on many single-crystal metal surfaces (Co, Ru, Rh, Ni) even when metal atoms are present as strained or distorted overlayers on oriented substrates (*41*).

The structure-insensitive nature of CO hydrogenation on Co is consistent with the similar turnover rates recently reported on Co single crystals with different exposed crystal planes (*42, 43*). Turnover rates on crystals with Co(11$\bar{2}$0) (zigzag grooved surface) and Co(0001) (close-packed surface) orientation differ only by about a factor of two; activation energies are similar on the two surfaces. The chain growth probability on the close-packed surface is lower (α = 0.2) than on the zigzag surface (α = 0.36), apparently because rapid olefin hydrogenation on the close-packed surface prevents olefin readsorption reactions that lead to the higher α values on Co(11$\bar{2}$0). This lack of structure sensitivity is particularly surprising because CO chemisorbs molecularly on Co(0001) between 100 and 450 K but dissociates readily above room temperature on Co(11$\bar{2}$0) (*44–46*). These data show that the effect of local surface structure on CO chemisorption disappears at the high steady-state CO surface coverages that exist during catalysis. These data also suggest that dissociative chemisorption of CO on Co(0001) occurs readily at 473–523 K during CO hydrogenation, perhaps because coadsorbed hydrogen adatoms increase the rate of CO dissociation steps (*15*).

Previously reported dispersion effects on Co catalysts were obtained at conditions that favor the formation of light products. In our study, we have extended this work to Fischer–Tropsch synthesis conditions (2000 kPa, 473 K) where C_5+ selectivities exceed 80%. We conclude that the synthesis of such higher molecular weight hydrocarbons depends only weakly on Co dispersion and on the identity of the metal oxide support. This conclusion is consistent with the small changes in surface structure that occur in the Co dispersion range studied here (0.0045–0.95) and from the weak electronic modifications expected from contact between crystallites in this size range (10–210 nm) and a metal oxide support (*2, 34*).

We cannot rigorously establish the structure-sensitivity of this reaction on Co because of the limited dispersion range studied. We conclude instead that the Fischer–Tropsch synthesis is unaffected by small structural changes that occur as Co crystallite size varies between 10 and 210 nm. We also suggest that the previously reported marked changes in turnover rate or selectivity in similar ranges of crystallite size cannot reflect structural effects on surface chemistry. Thus, our results, although not surprising, are reassuring, in view of the wide range of contradicting evidence previously reported on dispersion and support effects on CO hydrogenation rate and selectivity.

D. Dispersion and Support Effects on Fischer–Tropsch Synthesis Selectivity

Selectivity differences among catalysts reflect a complex interplay of intrapellet diffusion with readsorption and chain initiation by α-olefins, processes that are influenced by changes in support structure and metal loading and dispersion. The details of reaction–transport models required to describe these effects have been previously described (*5–8*). Here, we show how these models can explain changes in C_5+ selectivity that occur with changes in dispersion or support, without requiring modifications of the intrinsic surface kinetics of chain growth and termination. The results are illustrated here for Co catalysts but apply also to Ru catalysts, as we have shown previously (*5, 7*).

α-Olefins readsorb and initiate surface chains during FT synthesis. This secondary reaction effectively reverses the β-hydrogen abstraction step that terminates surface chains as α-olefins. As a result, readsorption reactions increase chain growth probability and product molecular weight without altering chain growth surface kinetics. The extent of olefin readsorption depends on the readsorption rate constant; in turn, surface chain growth and readsorption kinetics depend on the chemical properties and size of available surface metal ensembles and on electronic or structural perturbations caused by changes in support or in crystallite size. Our model relates C_5+ selectivity to structural support parameters and to the density of Co sites, properties that change with support and metal dispersion and which control the rate of readsorption of reactive olefins within catalyst pellets. In effect, the intrapellet residence time of olefins, and the number of readsorption sites with which they can interact as they diffuse, control the extent of readsorption and the C_5+ selectivity.

The intrapellet residence time of α-olefins depends on pellet size (L) and on the olefin diffusivity in the liquid reaction products; the latter is independent of pore size or support identity because diffusion occurs through liquid-filled pores, where diffusivities are independent of pore radius (r_p); the effective diffusivity depends on the tortuosity (τ) and on the pellet void fraction (ϕ), but such structural properties vary only slightly among the supports used in this study (*47*). The probability that a diffusing olefin will interact with an active site depends on the density of Co surface atoms on the support surface (θ, sites-m^{-2}) and on the specific support surface area (s, m^{-1}).

The combined effects of intrapellet residence time and site density can be included in a structural parameter (χ) that contains all structural catalyst properties influencing olefin readsorption (*5–7*):

$$\chi = \frac{L^2 \cdot \theta \cdot \phi}{r_p} \qquad (6)$$

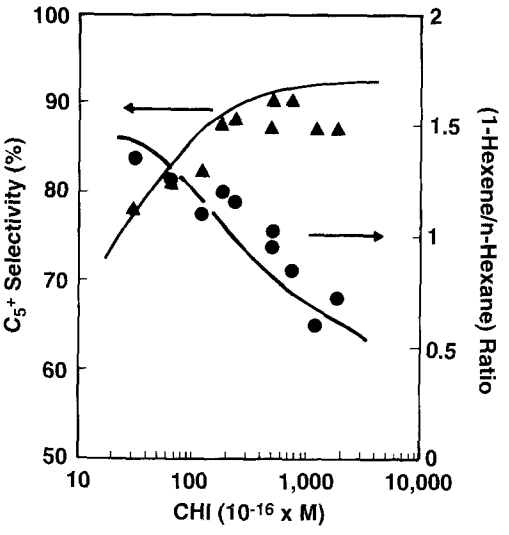

FIG. 5. Effects of catalyst structural properties and site density on C_5+ Selectivity (Experimental: Co on SiO_2, TiO_2, and Al_2O_3 supports; 473 K, H_2/CO = 2.1, 2000 kPa, 50–60% CO conversion; Model: solid line (*6, 7*)).

The ability to describe Fischer–Tropsch synthesis selectivity on Co catalysts using just this parameter implies that only the physical structure varies with changes in support or Co dispersion and that intrinsic catalytic and chemisorptive properties remain unperturbed by these changes.

C_5+ selectivity increases with increasing values of the structural parameter (χ), regardless of whether χ is changed by varing the support, or the metal dispersion or loading (Fig. 5). The increase in C_5+ selectivity reflects the higher intrapellet residence time and readsorption site density as χ increases. The solid curve in Fig. 5 was obtained from model simulations in which the intrinsic chain growth kinetics were kept constant in the solution of the reaction–transport model equations (*5, 6*). The excellent agreement between the model and the data suggests that selectivity differences normally attributed to variations in metal dispersion and in support chemical identity reflect instead changes in the extent of α-olefin readsorption. Indeed, the olefin content in synthesis products decreases with increasing χ because α-olefins are selectively consumed in

readsorption and chain initiation (not hydrogenation) reactions (Fig. 5) (*5, 6*). Changes in metal dispersion, support, or χ values do not affect the asymptotic ($C_{20}+$) chain growth and termination rates on Co surfaces; therefore, the catalytic properties of chain growth sites are unaffected by dispersion or support effects. Values of χ greater than those reported in Fig. 5 lead to lower C_5+ selectivity because of transport restrictions on CO hydrogenation rates within pellets with large diameter and active site density (*5–7*). Such transport restrictions lower CO concentration within catalyst pellets and lead to lighter and more paraffinic products. The diffusivity of CO in hydrocarbon liquids is much higher than that of large α-olefins; therefore, intrapellet CO transport restrictions occur at higher χ values than diffusion-enhanced α-olefin readsorption (*5–7*).

IV. CONCLUSIONS

The intrinsic catalytic activity of Co and Ru surface atoms is not strongly influenced by the size of the metal crystallites or by the identity of the metal oxide support. Site-time yields are similar on metal particles a widely different dispersion (Ru, 0.0009–0.60; Co, 0.0045–0.095) supported on TiO_2, SiO_2, Al_2O_3, and other supports. The carbon number distribution, the C_5+ selectivity, and the olefin content in products vary slightly with changes in dispersion and support. These effects reflect diffusion-enhanced readsorption of α-olefins, the extent of which depends on the physical structure of the support and on the density of exposed metal atoms within pellets. Diffusion-enhanced secondary reactions cannot be prevented even on small pellets because the liquid phase within the pores restricts the removal of products during the synthesis of heavy hydrocarbons on Co and Ru catalysts. Intrinsic chain growth kinetics are not affected by changes in support or dispersion, suggesting that surface reactions, adsorbed intermediates, and site activity are independent of metal particle size and of oxide support, at least for the supports and metal dispersion range reported here.

Our study extends previous studies of CO hydrogenation to conditions that favor the formation of high molecular weight hydrocarbons. We conclude that the Fischer–Tropsch synthesis is structure-insensitive on Ru catalysts. The range of metal dispersion in Co catalysts was too limited to satisfy the rigorous definition of structure-insensitivity (*34, 35*) because surface structure does not depend strongly on crystal size in this limited dispersion range (*2*). However, the constant site activity on all supports over this dispersion range and the mechanistic and kinetic resemblance of the Fischer–Tropsch synthesis on Co and Ru catalysts suggest that this reaction is structure-insensitive also on Co.

ACKNOWLEDGMENTS

We thank Dr. Sebastian C. Reyes for the model simulations shown in Fig. 5 and for his many independent contributions to our understanding of transport effects in Fischer–Tropsch synthesis. We also acknowledge the expert technical assistance of Mrs. Hilda Vroman and Messrs. Joseph E. Baumgartner and Bruce DeRites in the synthesis and catalytic evaluation of the cobalt catalysts reported here. Finally, we acknowledge Dr. Rostam J. Madon for many helpful discussions and insights and for his pioneering contributions to our knowledge of Fischer–Tropsch catalysis.

REFERENCES

1. Fischer, F., and Tropsch, H., *Brennst. Chem.* **13,** 61 (1932); Fischer, F., *Brennst. Chem.* **16,** 6 (1935).
2. van Hardeveld, R., and Hartog, F., *in* "Advances in Catalysis and Related Subjects", Vol. 22, p. 75. Academic Press, New York, 1972.
3. Tauster, S. J., and Fung. S. C., *J. Catal.* **55,** 29 (1978).
4. Madon, R. J., Bucker, E. R., and Taylor, W. R., NTIS Report No. FE8008-1, 1977.
5. Iglesia, E., Reyes, S. C., and Soled, S. L., *in* "Computer Aided Design of Catalysts and Reactors" (C. J. Pereira and E. R. Becker, Eds.) Dekker, New York, 1992, in press.
6. Iglesia, E., Reyes, S. C., Madon, R. J., and Soled, S. L., *in* "Advances in Catalysis and Related Subjects." Academic Press, New York, 1992, in press.
7. Iglesia, E., Reyes, S. C., and Madon, R. J., *J. Catal.* **129,** 238 (1991).
8. Madon, R. J., Reyes, S. C., and Iglesia, E., *J. Phys. Chem.* **95,** 7795 (1991).
9. Post, M. F. .M. and van Erp, W. A., European Patent Application 0 398 420 (1990); Netherlands

Patent Application 8,301,922 (1984), assigned to Shell.
10. Soled, S. L. and McVicker, G. B., *Prepr.—Am. Chem. Soc. Div. Pet. Chem.* **34**(3), 645 (1989).
11. Innes, W. B., *in* "Experimental Methods in Catalytic Research" (J. R. Anderson, Ed.), p. 45. Academic Press, New York, 1968.
12. Bartholomew, C. H., and Farrauto, R. J., *J. Catal.* **45,** 41 (1976).
13. Zwotiak, J. M., and Bartholomew, C. H., *J. Catal.* **82,** 230 (1983); *J. Catal.* **83,** 107 (1983).
14. Bartholomew, C. H., *Catal. Lett.* **7,** 27 (1990).
15. Biloen, P., Helle, J. N., and Sachtler, W. M. H., *J. Catal.* **58,** 95 (1979).
16. Brady, R. C., and Pettit, R., *J. Am. Chem. Soc.* **102,** 6181 (1980)
17. Flory, P. J., *J. Am. Chem. Soc.* **58,** 1877 (1936).
18. Friedel, R. A., and Anderson, R. B., *J. Am. Chem. Soc.* **72,** 1212 (1950); **72,** 2307 (1950).
19. Herrington, E. F. G., *Chem. Ind.,* 347 (1946).
20. Dalla-Betta, R. A., Piken, A. G., and Shelef, M., *J. Catal.* **51,** 386 (1978).
21. King, D. L., *J. Catal.* **51,** 386 (1978).
22. Kellner, C. S., and Bell, A. T., *J. Catal.* **75,** 251 (1982).
23. Smith, K. J., and Everson, R. C., *J. Catal.* **99,** 349 (1986).
24. Kelley, R. D., and Goodman, D. W., *Prepr. Pap.—Am. Chem. Soc. Div. Fuel Chem.* **25**(2), 43 (1980).
25. Kelzenberg, J. C., and King, T. S., *J. Catal.* **126,** 421 (1990).
26. Peden, C. H. F., and Goodman, D. W., *Ind. Eng. Chem. Fundam.* **25,** 58 (1986).
27. Bond, G. C., and Turnham, B. D., *J. Catal.* **45,** 128 (1976).
28. Luyten, L. J., van Eck, M., van Grondelle, J., and van Hooff, J. H., *J. Phys. Chem.* **82,** 2000 (1978).
29. Vannice, M. A., and Garten, R. L., *J. Catal.* **63,** 255 (1980).
30. Kikuchi, E., Matsumoto, M., Takahashi, T., Machino, A., and Morita, Y., *Appl. Catal.* **10,** 251 (1984).
31. Stoop, F., Verbiest, A. M. G., and Van der Wiele, K., *Appl. Catal.* **25,** 51 (1986).
32. Mims, C. A., Krajewski, J. J., Rose, K. D., and Melchior, M. T., *Catal. Lett.* **7,** 119 (1990).
33. Iglesia, E., and Boudart, M., *J. Phys. Chem.* **90,** 5272 (1986); **95,** 7011 (1991).
34. Boudart, M. and Djega-Mariadassou, G., "Kinetics of Heterogeneous Catalytic Reactions." Princeton Univ. Press, Princeton, NJ, 1984.
35. Boudart, M., *in* "Advances in Catalysis and Related Subjects," Vol. 20, p. 153. Academic Press, New York, 1969.
36. Ho, S. W., Hovalla, M., and Hercules, D. M., *J. Phys. Chem.* **94,** 6396 (1990).
37. Bartholomew, C. H., and Reuel, R. C., *Ind. Eng. Chem. Prod. Res. Dev.* **24,** 56 (1985); *J. Catal.* **85,** 78 (1984).
38. Fu, L., and Bartholomew, C. H., *J. Catal.* **92,** 376 (1985).
39. Rameswaran, M., and Bartholomew, C. H., *J. Catal.* **117,** 218 (1989).
40. Lee, J. H., Lee, D. K., and Ihm, S. K., *J. Catal.* **113,** 544 (1988).
41. Johnson, B. G., Bartholomew, C. H., and Goodman, D. W., *J. Catal.* **128,** 231 (1991).
42. Geerlings, J. J. C., Zonnevylle, M. C., and de Groot, C. P. M. *Surf. Sci.* **241,** 302 (1991).
43. Geerlings, J. J. C., Zonnevylle, M. C., and de Groot, C. P. M. *Surf. Sci.* **241,** 315 (1991).
44. Bridge, M. E., Comrie, C. M., and Lambert, R. M., *Surf. Sci.* **67,** 393 (1977).
45. Prior, K. A., Schwaha, K., and Lambert, R. M., *Surf. Sci.* **77,** 193 (1978).
46. Papp, H., *Surf. Sci.* **129,** 205 (1983); *Surf. Sci.* **77,** 193 (1978).
47. Reyes, S. C., and Iglesia, E., *J. Catal.* **129,** 457 (1991).